Friction Reduction through Ultrasonic Vibration Part 1: Modelling Intermittent Contact

Eric Vezzoli, Zlatko Vidrih, Vincenzo Giamundo, Betty Lemaire-Semail,

Frédéric Giraud, Tomaz Rodic, Djordje Peric, Michael Adams

▶ To cite this version:

HAL Id: hal-01629239
https://hal.inria.fr/hal-01629239

Submitted on 13 Nov 2017

Friction Reduction Through Ultrasonic Vibration: Part 1: Modelling Intermittent Contact

Eric Vezzoli, Zlatko Vidrih, Vincenzo Giamundo, Betty Lemaire-Semail, *Member, IEEE,*
Frederic Giraud, *Member, IEEE,* Tomaz Rodic, Djordje Peric, and Michael Adams

Abstract—Ultrasonic vibration is employed to modify the friction of a finger pad in way that induces haptic sensations. A combination of intermittent contact and squeeze film levitation has been previously proposed as the most probable mechanism. In this paper, in order to understand the underlying principles that govern friction modulation by intermittent contact, numerical models based on finite element (FE) analysis and also a spring-Coulombic slider are developed. The physical input parameters for the FE model are optimised by measuring the contact phase shift between a finger pad and a vibrating plate. The spring-slider model assists in the interpretation of the FE model and leads to the identification of a dimensionless group that allows the calculated coefficient of friction to be approximately superimposed onto an exponential function of the dimensionless group. Thus, it is possible to rationalise the computed relative reduction in friction being (i) dependent on the vibrational amplitude, frequency, and the intrinsic coefficient of friction of the device, and the reciprocal of the exploration velocity, and (ii) independent of the applied normal force, and the shear and extensional elastic moduli of the finger skin provided that intermittent contact is sufficiently well developed. Experimental validation of the modelling using real and artificial fingertips will be reported in part 2 of this work, which supports the current modelling.

Index Terms—Tactile devices and display, Tactile stimulator, Squeeze film effect, Ultrasonic devices, Friction modulation, Intermittent Contact, Coulombic Friction.

✦

1 INTRODUCTION

MOST current touchscreen consumer devices, such as smartphones and tablets, lack credible haptic feedback. The vibration of the whole device is able to provide some cues to users, but it is not capable of reproducing a natural tactile sensation. Different approaches to such texture reproduction are currently being investigated, e.g. lateral vibrations, ultrasonic vibrations and electrovibration. The former involves in-plane vibrations that are applied in an attempt to reproduce the vibrotactile modulation induced by a real texture [1]. The latter two approaches aim to modulate the perceived friction between a finger pad and the screen surface. The possibility of tracking the position of the fingertip led to a generation of spatio-temporal relationships that are useful for textural reproduction [2]. Systems exploiting electrovibration and ultrasonic vibration are two of the leading tactile feedback technologies, which are based on frictional modulation and which are being developed and coupled with capacitive touch screens. The first depends on the polarization of the finger pad by a high voltage supplied plate covered with an insulator [3], [4]. The resulting attractive force induces an increased frictional force when interacting with the display. The latter involves out-of-plane vibrations that attenuate the frictional force of a contacting finger pad. The effects of these two approaches are similar and they are perceived in the same manner [5]. Although the application of ultrasonic vibration is widely studied, it is still not fully understood in terms of the possible mechanisms that can lead to frictional modulation and hence device design optimisation is difficult without a reliable theoretical or numerical model. Currently, the most widely accepted explanation involves aerodynamic levitation by the *squeeze film* effect [6], [7], which would directly lead to a reduction in the friction by completely or partially reducing the extent of finger-display interaction. However, there is a discrepancy between the measured frictional force as a function of the vibrational amplitude at large amplitudes ($\sim 2\,\mu m$), and what would be expected on the basis of squeeze film levitation [8]. Moreover, it has been established by direct measurement that there is intermittent mechanical contact between a finger pad and an ultrasonic vibrating plate [9], [10], [11], which suggest the possible contribution of a mechanical interaction firstly outlined by Biet et al. [12] The aim of the current work is to re-examine the role of the squeeze film effect and intermittent contact in the friction modulation induced by ultrasonic vibration. It will be described in two parts. Part 1 will examine in depth the mechanical interaction between a finger pad and the vibrating plate, which suggests a mechanical explanation of the reduction of friction, whereas part 2 will provide experimental assessment of the proposed model and of the contribution of the squeeze film effect to the reduction of friction.

- *E. Vezzoli, B. Lemaire-Semail and F. Giraud are with Univ. Lille, Centrale Lille, Arts et Metiers ParisTech, HEI, EA 2697 - L2EP - Laboratoire d'Electrotechnique et d'Electronique de Puissance, F-59000 Lille, France E-mail: eric.vezzoli@ed.univ-lille1.fr, betty.semail@polytech-lille.fr, frederic.giraud@polytech-lille.fr*
- *Z. Vidrih and D. Peric are with Swansea University, College of Engineering, Zienkiewicz Centre for Computational Engineering, Bay Campus, Swansea SA1 8EN, United Kingdom E-mail: z.vidrih@swansea.ac.uk, d.peric@swansea.ac.uk*
- *V. Giamundo, and T. Rodic are with C3M d.o.o., Centre for Computational Continuum Mechanics, Tehnoloski Park, 21, SI1000, Ljubljana, Slovenia E-mail: vincenzo.giamundo@c3m.si, tomaz.rodic@c3m.si*
- *M. Adams is at the School of Chemical Engineering, University of Birmingham, Edgbaston, B15 2TT, United Kingdom Email: m.j.adams@bham.ac.uk*

In part 1, the experimental studies by Dai et al. [9], involving the measurement of intermittent contact of a finger pad at two different vibrational amplitudes using an optical technique, will be extended to a full characterisation of the entire relevant vibrational amplitude range. The data will be employed for calibration and validation of a finite element (FE) model that is developed in order to investigate how intermittent contact would act to reduce the friction. It will be shown that simply reducing the time of contact is not a sufficient criterion. Indeed, for a Coulombic slider with a constant coefficient of friction, if contact is detached intermittently under quasi-static conditions, the mean frictional force will scale as the fraction of the sliding time in contact. However, if the slider is vibrated at high frequencies with periodic detachment, it is reasonable to expect that a steady state normal force balance will be maintained and thus, for a Coulombic slider, the mean frictional force cannot simply be computed from the fractional contact time. For the general case, it is difficult to establish theoretically that such a force balance would be satisfied. Thus this force balance is demonstrated to be valid for the considered system by an implementation of the FE model.

The material constants for the FE model were optimised against the optical data by the application of an inverse method. In addition, the analysis was implemented for a large parametric space and thus it was computationally too expensive to employ a full 3D structural model of a finger pad. However, the longest relaxation time for a finger pad measured under normal loading is $\sim$ 3 s [13], which is orders of magnitude longer than the timescale of tens of μs for ultrasonic vibration. Thus it may be assumed that the inner soft tissues of a finger pad are effectively immobile when periodically loaded at a high frequency i.e. the viscoelastic retardation time governing unloading is much longer than the period of vibration. It follows that the high frequency response may be approximated as being localised in the more elastic skin layers, which were modelled in 2D.

FE modelling should lead to a quantitative simulation of a given system that corresponds to experimental measurements with the advantage that all field data, e.g. forces, displacements and velocities, are directly accessible. However, as in the case of experiments, such models lead to particular rather than general solutions that are more useful for design engineers. Consequently, on the basis of the friction reduction mechanism identified by the FE model, a simplified spring-slider model was developed. It allowed a dimensionless group to be developed that incorporated the critical design, operational and user variables that govern the performance of an ultrasonic haptic display. While such models cannot lead to quantitative predictions of the performance, it was possible to develop an empirical relationship between the dimensionless group and the performance.

In part 2, [14], experimental data will be described showing that a decrease in the ambient pressure does not influence the reduction in friction induced by ultrasonic vibration. This was for a limited set of experimental conditions but it does support the contention that the recurrent loss in contact is a contributing mechanism. Furthermore, frictional data for human and artificial fingertips sliding on an ultrasonic plate are reported that are consistent with both the FE and spring-slider models.

2 SKIN-PLATE CONTACT DYNAMICS

2.1 Description of the Experimental Setup

The experimental equipment developed to measure the dynamics of the finger pad-plate contact in the ultrasonic domain is shown Fig. 1. The aim was to record the local velocity of the fingerprint ridges while in periodic contact with the ultrasonically vibrating plate. This was achieved using a laser Doppler vibrometer (OVF-5000, Polytech, Germany) that was focused on the surface of the finger pad across a transparent vibrating plate. The diameter of the laser focus spot was 120 μm, which is comparable with that of a fingerprint ridge ($\sim$ 300 μm); the ridges were coloured with reflective paint to enhance the signal-to-noise ratio. The procedure is similar to that described in [9]. The applied normal force between the finger and the plate was recorded by a force sensor (nano43, ATI, USA) mounted beneath the plate holder. The height of the whole structure could be adjusted using two micro-positioners (M-SDS40, Newport, USA) in order to control the normal force with an angle between the finger and the plate of 45°. The vibrational amplitude of the plate and the surface velocity of the fingerprint ridges were monitored by an oscilloscope (3014B, Tektronix, USA) and the applied force was acquired simultaneously through serial communication with a computer.

2.2 Measurement Protocol

The measurements were performed on the index finger of a male subject (age 26 years) who gave his informed consent. For each acquisition, the plate was cleaned with alcohol, and the finger washed with commercial soap, rinsed with water and dried with absorbent paper. There was a minimum delay of 3 min before performing any measurements to allow the finger and plate to equilibrate. The mean moisture content of the finger pad was 35 a.u. as measured with a Corneometer (CM 825, Courage + Khazaka electronic GmbH, Germany); this is defined as the moist condition. Dry condition was achieved by washing the finger pad with acetone using a similar procedure described previously [15], [16]. The dynamic behaviour of the skin in contact with the plate was recorded for different peak-to-peak amplitudes in the range 0 - 2.5 μm, which is generally implemented in ultrasonic displays [8]. The applied normal force on the finger was 0.25 $\pm$ 0.05 N. The required amplitude of vibration of the plate was initiated before contact with the finger pad was made, which was for a duration of 20 s. The measurements were performed multiple times for the two different moisture conditions of the finger. Every experimental point corresponds to 10 measurements in order to ensure the repeatability of the results.

2.3 Experimental Results

Typical experimental data for the displacement, velocity and acceleration of the finger pad and plate at peak-to-peak vibrational amplitudes of 0.42, 1.35 and 2.5 μm are presented in Fig. 2. The displacement values are calculated from the integration of the velocity measurements as a function of time, and thus it is not possible to specify an absolute value of the detachment time; the corresponding separation distances between the finger pad and plate are also shown.
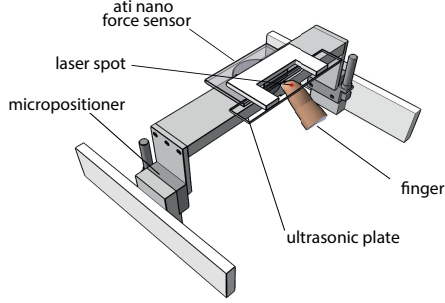
Fig. 1: Schematic diagram of the equipment used to measure the contact time between a finger pad and vibrating plate. The finger is inclined at an angle of $45°$ to the plate and the focus spot is visible on the skin surface.
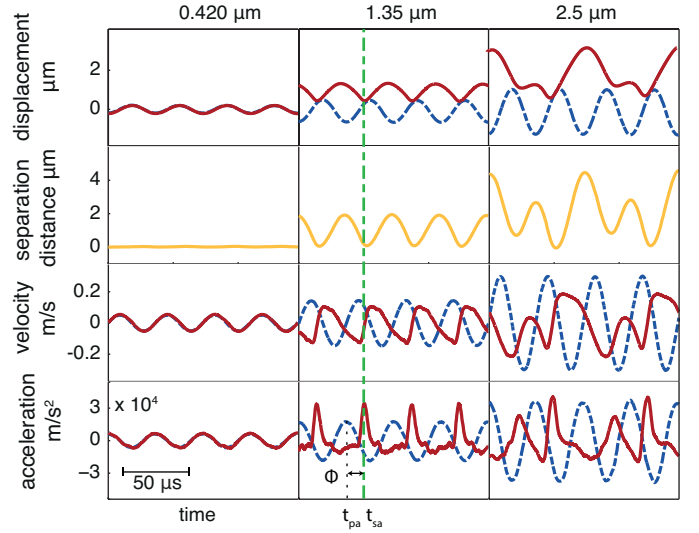

Fig. 2: Displacement, separation distance, velocity and acceleration of the skin of the finger pad in the dry condition (continuous lines) interacting with an ultrasonic vibrating plate for three peak-to-peak vibrational amplitudes of 0.420, 1.35 and 2.5 µm; the data for the plate are shown as dashed lines. The applied normal force between the finger pad and the plate is 0.25 N. The green vertical dashed line indicates the concomitance of the peak of the acceleration with the beginning of contact between the finger pad and the plate once the intermittent contact is established. The displacement of the skin is inferred by the velocity measurement of the interferometer vibrometer, and it is positive during the indentation of the skin.

At an amplitude of 0.42 µm, the data for the plate and finger pad are in phase with identical amplitudes so that contact is completely maintained; this has been referred to as the *sticking regime* [10]. There is a phase lag of $\sim 90°$ at an amplitude of 1.35 µm that is accompanied by a significant period for which the finger pad is not in contact with the plate; this has been referred to as the *bouncing regime* [10]. Similar measurements were reported in [11]. At the amplitude of 2.5 µm, the period of the finger displacement has doubled. The trends in the results may be quantified by calculating the phase shift $\Phi(w)$:

$$\Phi(w) = 360 \frac{|\, t_{pa}(w) - t_{sa}(w)\, |}{T} \quad (1)$$

where w is the amplitude of vibration, t_{pa} and t_{sa} are the times of the maximum acceleration of the plate and the skin of the finger pad respectively, and T is the vibrational period.

The origin of the phase shift may be understood by considering the behaviour corresponding to the vertical dashed line in Fig. 2 that intersects the peak in the acceleration of the skin as it is impacted by the plate. Following such an impact, the skin will continue to be displaced away from the plate as the plate retracts. Eventually, the stored elastic energy in the skin will cause it to unload and re-contact the plate. The greater peak acceleration at the amplitudes of 1.35 and 2.5 µm results in larger deformations and impact displacements of the skin and hence a greater phase shift. Both the velocity and acceleration peaks for the skin are asymmetric and this arises from significant retardation during unloading, which could arise from either viscoelastic damping or inertia, or a combination of both effects. The dependence of the phase shift on the vibrational amplitude is shown in Fig. 4a. It evolves from a low value, corresponding to full contact between the finger pad and plate, to a saturated mean value, corresponding to intermittent contact, under high vibrational amplitudes for both the dry and moist conditions.

3 FINITE ELEMENT MODEL

3.1 Introduction

To model the behaviour of the fingerprint ridges interacting with an ultrasonically vibrating plate, a FE model is developed. It was necessary to take into an account the different characteristics of the tissues, the viscosity of the materials, and the dynamic contacting phenomenon.

A 2D three domain linear viscoelastic model of a fingerprint ridge was generated to represent the three most external layers of the skin: the *stratum corneum*, *dermis* and subcutaneous tissues. Periodic boundary conditions were applied to the sides of the model in order to reproduce the periodicity of the fingerprint ridges on the human finger pad. A rigid boundary condition was set in the upper part of the model since the inner finger pad was considered to be immobile during the timescale of the vibrations as discussed in the introduction. The selected model parameters are presented in Table 1. The load applied on the single ridge was calculated by the mean pressure corresponding to an applied force of 0.25 N. The gross contact area was calculated according to the Hertz relation reported in [17], and rescaled on the 2D model. A schematic diagram of the implemented example together with the boundary conditions is shown in Fig. 3.

3.2 Implementation

The explicit solver version of the commercially available FE analysis software Elfen (Rockfield Software Ltd., Swansea, UK) was employed. Four-noded plane strain quadrilateral hourglass elements [21] with strain stabilization were utilized to discretise the geometry. These 2D continuum elements are based on the standard isoparametric approach
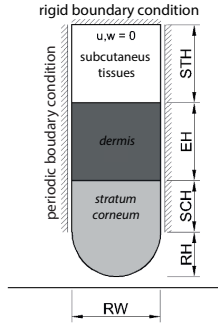
Fig. 3: Schematic representation of the FE model of a fingerprint ridge. RW is the width of the ridge, RH the height of the ridge, and SCH, EH and STH are the thicknesses of the *stratum corneum*, *dermis* and subcutaneous tissues. The representation is not in scale.

TABLE 1: Input material parameters for the FE model; common values of the Poisson's ratio, density and retardation time were assigned to the three domains of the skin [18], [19], [20].

Parameter	Description	Input Value or Optimization Range
RH	*stratum corneum* ridge height	200 µm
SCH	inner *stratum corneum* thickness	100 µm
EH	*dermis* thickness	600 µm
STH	subcutaneous tissues thickness	1800 µm
RW	width of the ridge	500 µm
μ_0	coefficient of friction without vibration	0.1 - 2.0
k	penalty parameter	(10-1000) E_{sc}
E_{sc}	Young's modulus of *stratum corneum*	10-1000 MPa
E_{ep}	Young's modulus of *dermis*	1.5 MPa
E_{ep}	Young's modulus of subcutanous tissue	0.02 MPa
G_{sc}	shear modulus	$E_{sc}/2(1+\nu)$
ν	Poisson's ratio	0.33
ρ	density	750 kg/m³
τ	retardation time	$0 - 10s$
ζ	Rayleigh damping	1
f	plate frequency	27500 Hz
w	plate amplitude	$0.05 - 2.5$ µm
F_n	normal force applied by the fingerpad	0.25 N

where the same shape functions are used to interpolate both the displacements and the geometry. The strain-displacement relationship was formulated using a velocity-strain measure, from which the incremental strains were evaluated. The elements use one-point integration, consequently the four-noded elements have stabilization terms to limit zero-energy or hourglass deformations. The elements also utilise an artificial bulk viscosity to smooth shock discontinuities that may occur during impact problems. The contact between the skin and the plate was modelled using the penalty method with Coulombic friction [22], where the plate was assumed to be rigid in comparison with the fingerprint ridge. The penalty method is based on the introduction of an inertia free element at the boundaries to smooth the contacts between the bodies and prevent overlap between the elements. The Coulombic boundary condition was applied globally rather than locally and thus the ridge may be regarded as having a sufficiently fine-scale roughness that it exhibits Hertzian deformation to a close approximation [23]. If the boundary condition was applied locally, the ridge would exhibit the characteristics of a smooth Hertzian contact such that the coefficient of friction would decrease with increasing normal force [24]. The influence of the penalty parameter, k, was investigated for optimisation purposes since it introduces an additional stiffness in the dynamic model. It was estimated that for $k > 80E_{sc}$, its influence on the model dynamics is negligible. The viscoelastic properties of the skin were parameterized by a retardation time, τ. The analyses were implemented in parallel with a Matlab code on multiple cores of a desktop computer (Intel i7 Six Core Processor, 3.4 GHz, and 16 GB RAM, DDR3 2400 MHz). Matlab was used to generate the input files for Elfen and for reading and post-processing the output files.

3.3 Inverse Analysis

The complex nature of biological tissues results in a huge variability in the mechanical properties of the skin. Moreover, FE modelling requires additional numerical parameters that are not physically related. In order to find reliable model parameters that lead to an accurate simulation of the experimental phenomena, an inverse modelling procedure was adopted [25], [26], [27]. In particular, the procedure aims to identify a set of parameters that, according to the chosen accuracy, allows the numerical model to fit the experimental behaviour. Here, the fitted parameters were the viscoelastic behaviour of the model (the retardation time), and the Young's modulus of the *stratum corneum* to reproduce the two conditions experimentally studied. The values of the material parameters and the allowed fitting range are reported in Table 1 referred to Fig. 3. The fitted parameters are highly variable or unknown in the ultrasonic range. Moreover, the k parameter, which has no physical meaning, is also fitted, but it has to fulfill the requirements previously expressed. This goal is achieved by minimizing a function (i.e. an objective function) that returns the difference between the experimental and the numerical data (i.e. the misfit). At the end of the procedure, the fitted Young's modulus of the *stratum corneum* was compared with literature [19] values to assess the validity of the developed model for both the moist and dry cases. The phase shift parameter, Φ, was selected as a fitting function since it effectively characterises the skin behaviour as a function of the vibrational amplitude. The objective function to be minimised is:

$$\text{Objective} = \sum_{i=1}^{N} \left[\Phi(w)^{FEM}(E_{sc},k,\tau) - \Phi(w)^{expt} \right]^2 \quad (2)$$

where N is the number of experimental points included; $\Phi(w)^{FEM}(E_{sc},k,\tau)$ is the phase shift calculated at the amplitude w and $\Phi(w)^{expt}$ is the experimental phase shift

TABLE 2: Inverse Analysis Results, in brackets the comparison of the literature value [19]

Parameter	Description	Moist (MPa)	Dry (MPa)
E_{sc}	Young's modulus of *stratum corneum*	28 (10 - 50)	202 (70 - 1000)
τ	retardation time	0 s	0 s
k	penalty parameter	93 MPa	144 MPa

measured at the same amplitude. The model was implemented with an initial dwell time between the finger pad and plate, t_{press}, then held in position until a time, t_{on}, when the vibrational amplitude of the plate was increased to the first value assumed in the experimental evaluation and maintained for a time, t_{step}. The dynamics of the contact nodes in terms of displacements, velocity and accelerations were recorded in output files and post-processed to calculate the phase shift, Φ, for a given amplitude using Eq. (1). The procedure was repeated for all vibrational amplitudes measured to compute $\Phi(w)^{FEM}(E_{sc}, k, \tau)$ for a given set of parameters. Then, the objective function was evaluated and the procedure was terminated in case of convergence or repeated with a different set of parameters.

The convergence parameters obtained by the inverse analysis method for both finger pad moisture contents are reported in Table 2. For both moist and dry condition, the identified value of the *stratum corneum* stiffness falls in the accepted range of literature data in quasi-static condition [19]. For both skin conditions, it was found that the retardation time did not significantly affect the results. Consequently, the simple elastic case ($\tau = 0$) was selected. The comparison between experimental and simulated phase shift data for the best-fit parameters is reported in Fig. 4a and the surface profile of the phase shift as a function of the vibrational amplitude and the Young's modulus of the *stratum corneum* is shown in Fig. 4b. The comparison between the experimental data and those calculated by the FE analysis using the optimised data for the dry case and the vibrational amplitude of 1.35 μm is illustrated in Fig. 5; the trends are similar for the moist case. In the case of the measured data (Fig. 2), the asymmetry of the calculated velocity peak is also evident. Since the model is elastic rather than viscoelastic the asymmetry is due to inertia only; in the absence of inertial retardation the linear sloping component of the unloading phase would be horizontal. The difference between the measured and modelled data arises by the reporting of the velocity of one node of the model, whereas the measured data is the result of integrating along all the area of the ridge.

3.4 Results of the Finite Element Analysis in Sliding Conditions

The previous paragraphs allowed the parameterization of the FE model based on experimental data, in this section the model will be used to study the sliding condition.

To investigate the friction between the ultrasonically vibrating plate and the fingerprint model, the following procedure was adopted: (i) from 0 to t_{press} a constant normal load is applied to the finger pad as a boundary condition, the contact with the plate is fully established, and it is allowed to stabilise until $t = t_{slide}$, (ii) an additional boundary condition is then imposed corresponding at $t = t_{slide}$ corresponding to a lateral velocity, U, and (iii) at $t = t_{on}$ the plate is vibrated with a given amplitude, as shown in Fig. 6. Typical field and mesh distortion images with and without vibration are shown as a video in the supplementary material.

Fig. 7 shows the plate reaction force as a function of time for three vibrational amplitudes calculated by the FE model. The data are consistent with the measured values of the separation distances shown in Fig. 2. That is, at an amplitude of 0.1 μm, the force is always positive since the finger pad remains in contact with the plate. At an amplitude of 1 μm, there is a significant period when $F_{reac} = 0$ corresponding to a loss of contact. In addition, the maximum normal force exceeds the applied value and this arises because there are impacts between the plate and the finger pad, which is modelled as a fingerprint ridge of finite mass, as discussed in the context of the bouncing regime in section 2. The duration of non-contact increases at an amplitude of 2 μm and the maximum reaction force is also greater than at the amplitude of 1 μm. However, when calculating the integral mean value of F_{reac} over a vibration cycle, it is found to be constant for all three amplitudes and it is equal to the applied normal force of 0.25 N. For a quasi-static system, the integral mean normal force would simply scale with the fractional contact time. Fig. 2 shows that the acceleration has a maximum value during an impact so that the normal rebound force will be greater than the applied normal force due to inertia. That is, for this dynamic system. a normal force balance is satisfied and thus the integral mean of the coefficient of friction may be obtained from the following relationship:

$$\mu(w) = \frac{\int_t^{t+T} F_l(w)dt}{\int_t^{t+T} F_{reac}(w)dt} \tag{3}$$

The integral mean coefficient of friction, $\mu(w)$, derived from the FE simulations is calculated as the ratio of the mean values of the lateral force (friction force), F_l, and the normal force between the skin and the plate, F_{reac}, over a vibrational period T:

$$\int_t^{t+T} F_{reac}(w)dt = \int_t^{t+T} F_{reac}(0)dt \tag{4}$$

Thus the mean relative coefficient of friction, $\mu(w)' = \mu(w)/\mu_0$, can be calculated as:

$$\mu(w)' = \frac{\int_t^{t+T} F_l(w)dt}{\int_t^{t+T} F_{reac}(w)dt} \frac{\int_t^{t+T} F_{reac}(0)dt}{\int_t^{t+T} F_l(0)dt} = \frac{\int_t^{t+T} F_l(w)dt}{\int_t^{t+T} F_l(0)dt} \tag{5}$$

where μ_0 is the intrinsic coefficient of friction when $w = 0$. Fig. 8 shows (i) F_{reac} as a function of time for a single period from the data in Fig. 7 with an amplitude of 1.35 μm and (ii) the frictional force, $\mu_0 F_{reac}$, assuming that slip occurred directly after contact. However, the value calculated by the FE analysis is much less than $\mu_0 F_{reac}$ since when contact is made, the ridge deforms laterally rather than slips. The deformation is Hertzian so that initially, just after the contact, the lateral force is small since the contact
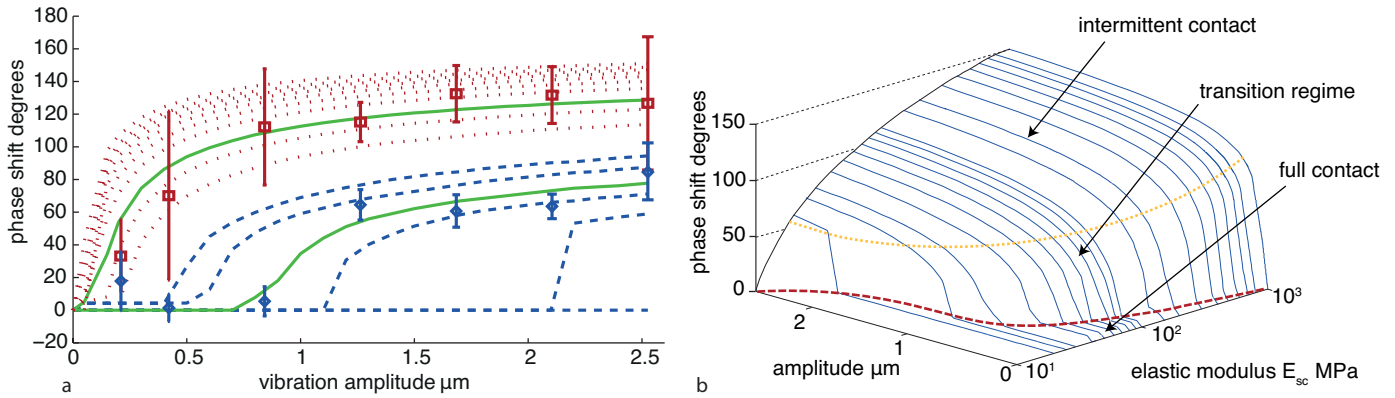
Fig. 4: (a) The measured phase angles as a function of the vibrational amplitude under dry (red squares) and moist (blue diamonds) conditions. The corresponding calculated values using the FE modelling are also shown as the blue dashed and red dotted lines respectively. Each line corresponds to a different value of the Young's modulus of the *stratum corneum* varying, for the moist condition, between 20 (lower line) to 50 MPa (upper line). The Young's modulus for the dry condition varies between 100 (lower line) to 1000 MPa (upper line) [19]. The continuous green lines are the best fits of the calculated values to the measured results and correspond to Young's moduli of 28.3 and 202.4 MPa respectively. (b) Phase shift as a function of the Young's modulus of the *stratum corneum* and the vibrational amplitude calculated by the FE analyses. The lowest region corresponds to continuous full contact between the finger pad and plate (sticking). The intermediate region refers to the transition phase, where the skin and the plate start to exhibit intermittent contact that is fully developed in the upper region (bouncing).
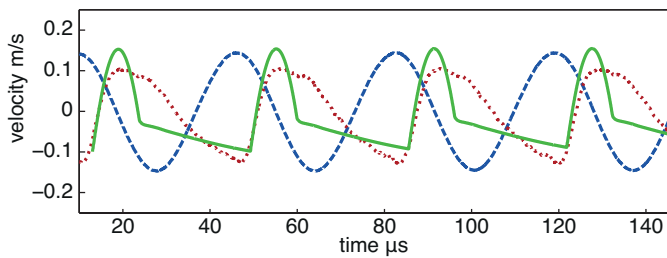

Fig. 5: Comparison between simulated (continuous green line) and measured (dotted red line) velocities of the finger print ridge (dry case) for a vibrational amplitude of 1.35 μm; the plate velocity is plotted as a dashed blue line; the velocity corresponds to one node at the base of the ridge.
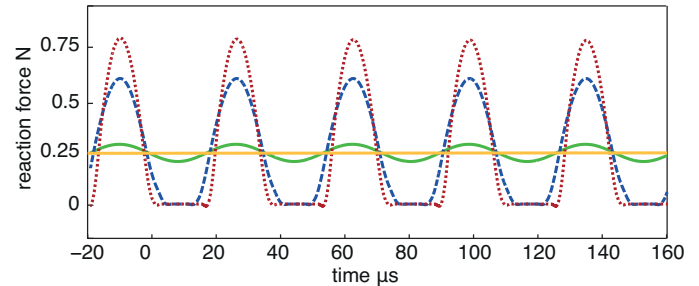

Fig. 7: Reaction force between the plate and the ridge calculated using the FE analysis under a normal force of 0.25 N applied without vibration (horizontal yellow line) and with different peak-to-peak vibrational amplitudes of 0.1 (continuous green line), 1 (dashed blue line) and 2 (red dotted line) μm.
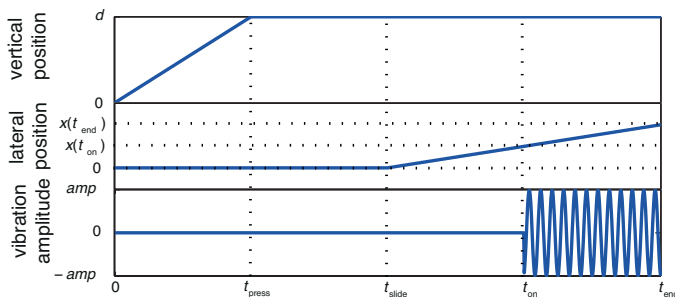

Fig. 6: Loading conditions for the FE examples.

area is small. With increasing normal load, the contact area increases and thus the lateral force increases until it is equal to $\mu_0 F_{reac}$, and then slip will be initiated. The subsequent time evolution of the lateral force is governed by $\mu_0 F_{reac}$, and the value slowly decreases until it becomes zero when contact is lost. The reduction of friction corresponds to the reduced area under the frictional curve represented in Fig. 8. To investigate the influence of the various parameters on the attenuation of the friction, multiple simulations were performed under the loading conditions represented in Fig. 6 as function of the vibration amplitude. The influence of the vibrational frequency, Young's modulus of the *stratum corneum*, the intrinsic coefficient of friction, normal load and exploration velocity on the frictional force were evaluated. The results of the parametric studies are shown in Fig. 9. The reduction in the friction is particularly sensitive to the vibrational frequency, intrinsic coefficient of friction and the sliding velocity. The origins of these trends will be considered in the next section assisted by a spring-slider model for interpreting the data.
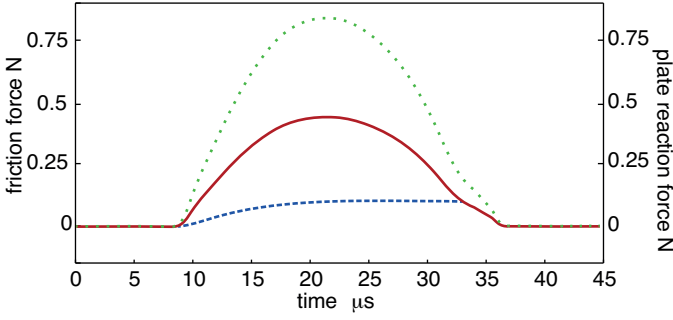
Fig. 8: FE results for the friction between a ridge in contact with an ultrasonic vibrating plate for one period of vibration. The dotted green line is the plate reaction force F_{reac}, the continuous red line is the value of $\mu_0 F_{reac}$ with μ_0= 0.5, and the dashed blue line is the lateral force acting on the ridge nodes in contact with the plate. The simulation has been carried for a vibrational amplitude of 1.35 μm, an applied normal force of 0.25 N and a sliding velocity of 20 mm/s.

4 SPRING SLIDER MODEL

4.1 Modeling

In this section, a simplified ideal elastic model is introduced to highlight the key elements underlying the friction reduction for ultrasonic devices. The mechanical principle may be interpreted by such a model based on a Coulombic slider attached to lateral and normal linear springs, with stiffnesses k_l and k_n respectively. The Coulombic slider may be considered simply as a block for which the coefficient of friction is independent of the applied normal force. As proposed in [30], the slider may be considered to represent a fingerprint ridge that is attached to a rigid finger pad. It is assumed that the static compression of the normal spring is less than that of the vibrational amplitude. If the slider has finite mass, this coupled spring system requires a numerical solution. However, the aim of the model is to provide a qualitative interpretation that facilitates an explanation of the underlying physics. Thus it is sufficient to treat the slider as having zero mass, which only influences the second order effects of inertia and overshoot. Given an applied normal force, F_n, between the slider and the plate, the normal preloading can be calculated as:

$$h = \frac{F_n}{k_n} \qquad (6)$$

When the plate is vibrating with a sinusoidal profile, the amplitude of vibration, w must be greater than h in order to induce the detachment of the spring. It is then possible to define a critical vibrational amplitude, w_c, corresponding to a normal force F_{nc}:

$$w_c = \frac{F_{nc}}{k_n} \qquad (7)$$

For $w < w_c$, the spring and plate are in full contact over the whole vibrational period, whereas for $w > w_c$ the contact is intermittent. At equilibrium, the mean integral of the imposed force by the normal spring must be equal to the total reaction force of the plate over a vibration cycle by analogy with Eq. (4):

$$\int_t^{t+T} F_{reac}(w)dt = \int_t^{t+T} F_{reac}(0)dt = F_n T \qquad (8)$$

where T is the period of vibration. For any given sliding velocity, U, the out-of-contact coefficient of friction is zero and it is equal to μ_0 when contact is made. Initially, after contact is re-established, the lateral displacement of the plate is accommodated by compression of the lateral spring and thus the frictional force will increase linearly with the compression until the spring force is equal to the frictional force. Thus slip will occur at a critical compression, Δx_c:

$$\Delta x_c(w,t) = \frac{\mu_0 F_{reac}(w,t)}{k_l} \qquad (9)$$

For a given vibrational amplitude, the time at which the slip occurs, t_s, can be defined as:

$$t_s = \frac{\Delta x_c(t_s)}{U} \qquad (10)$$

Provided that $t_c > t_s$, where t_c is the total contact time, it is possible to recover the frictional force as function of time, $F_l(t)$, for each vibrational period:

$$F_l(t) = U t k_l \quad \text{if} \quad 0 < t < t_s \qquad (11)$$

$$F_l(t) = \mu_0 F_{reac} \quad \text{if} \quad t_s < t < t_c \qquad (12)$$

$$F_l(t) = 0 \quad \text{if} \quad t_c < t < T \qquad (13)$$

The preloading of the lateral spring is removed when it detaches from the plate and thus it is fully unloaded when contact is re-initiated. The visualization of this simple model for an established intermittent contact is shown in Fig. 10 The periodicity of the contact generates the reduction in friction that is experienced while interacting with ultrasonic devices. This figure reproduces the trends calculated from the FE analysis shown in Fig. 8 except that the loading is linear rather than Hertzian. In order to be a realistic representation, the spring-slider model should be able to reproduce the measured trends in the vibrational amplitude dependence of the phase shift as shown in Fig. 5a. The plate reaction force was calculated for a single period as the sum of the elastic preloading of the normal spring, h, and the elastic force induced by the vibration of the plate:

$$F_{reac}(t) = k_n w \sin(2\pi f t) + k_n h \qquad (14)$$

such that $F_{reac}(t) > 0$ when the plate is in contact and $F_{reac}(t) = 0$ when the plate is out of contact. Eq. (8) may be written in the following form:

$$\int_0^{t_c} F_{reac}(t)dt = F_n T \qquad (15)$$

The integral in Eq. (15) was evaluated numerically for different values of h using the Newton-Cotes method until there was convergence to the value of the right-hand side. The time required for contact, t_c was determined by substituting the converged value of h in Eq (14) and this corresponds to that for the maximum acceleration of the slider. The phase shift was calculated from Eq. (1) with t_{sa} being the time of contact between the plate and the slider; the results are shown in Fig. 11. In order to obtain values that were
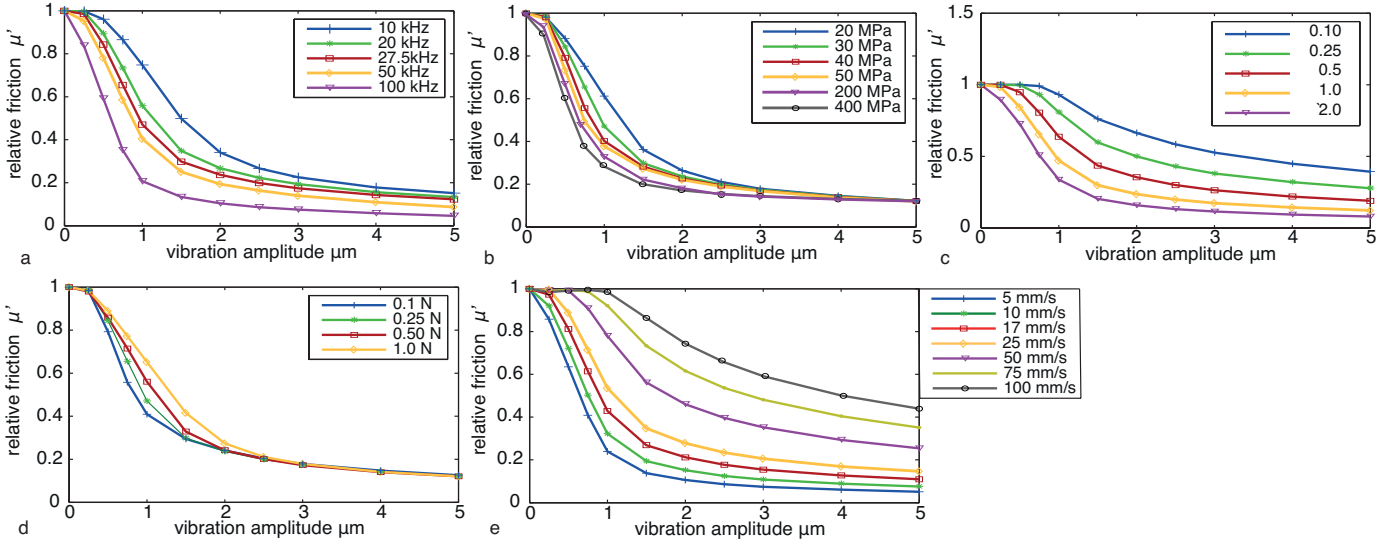
Fig. 9: The relative coefficient of friction as a function of the vibrational amplitude for a range of the following parameters: (a) vibrational frequency, (b) Young's modulus of the *stratum corneum*, (c) intrinsic coefficient of friction, (d) applied normal force, and (e) exploration velocity. These data were calculated by the FE analysis and, unless stated otherwise, the material input parameters are those identified through the inverse analysis for the moist case (Table 2); the exploration speed is 20 mm/s, the applied force is 0.25 N, $\mu_0 = 0.5$ and the vibrational frequency is 27.5 kHz.
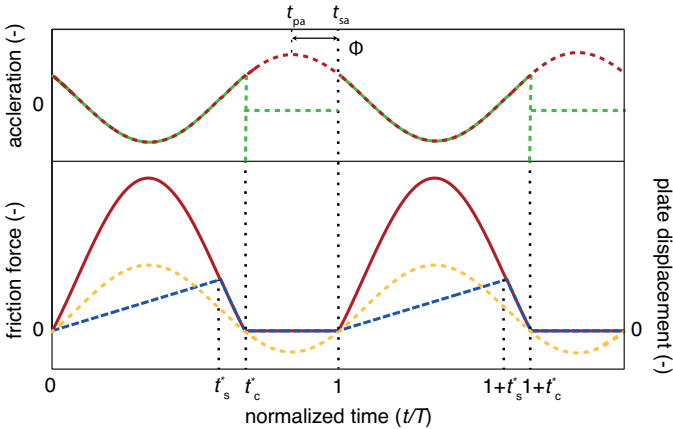

Fig. 10: Explanation of the reduced friction of an elastic body periodically in contact with a vibrating plate; the frictional force as a function of time was calculated using the spring-slider model where $t_s^* = t_s/T$ and $t_c^* = t_c/T$. The continuous red lines are determined by $\mu_0 F_{reac}$ i.e. the frictional force that would be generated if Coulombic slip occurred throughout each cycle. The dashed blue lines correspond to the lateral force on the elastic body at the interface with the vibrating plate. The dotted black vertical lines denote the duration for which there is Coulombic slip. The dashed red line is the acceleration of the plate as a function of time. The dashed green line is the acceleration of the elastic body, and the dashed yellow line is the plate displacement; the acceleration has a maximum value at a time just before it separates from the plate and then the value is instantaneous zero since the body has zero mass. The phase shift is defined as the lag of the peak acceleration of the elastic body relative to that of the plate.
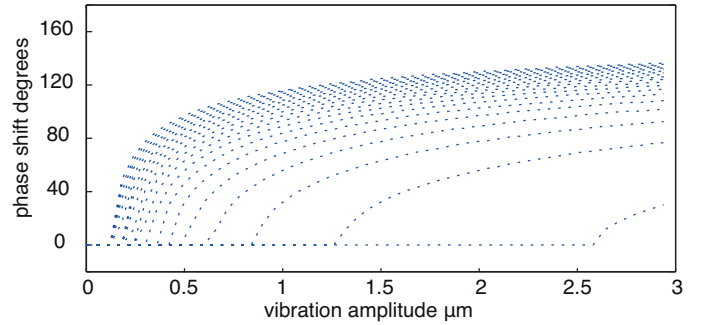

Fig. 11: Phase shift calculated using the spring-slider model for spring stiffnesses in the range from 0.2 (lower line) - 4 MN/m (upper line) for an applied normal force of 0.5 N.

comparable to those measured (Fig. 4), it was necessary to input a range of normal spring stiffnesses (0.2 - 4 MN/m) that is orders of magnitude greater than those measured ($\sim$ 2 kN/m) for the finger pad at much lower frequencies [28]. This reflects the much more rigid response at ultrasonic frequencies.

4.2 Parametric Analysis

For a given normal force, the static compression of the normal spring will increase with decreasing stiffness so that the value of t_c will increase since the unloading displacement will be greater. However, the lateral force depends on the shear elastic modulus of the *stratum corneum*, which is related to the Young's modulus by $G_{sc} = E_{sc}/2(1+\nu)$, the lateral stiffness scales with the normal value. Thus such an increase in t_c is partly compensated by a relative decrease in lateral stiffness that reduces the rate of increase of the lateral force and hence the integral frictional work. Fig. 9b suggests that this is approximately the case for

$w > 2.5$ µm, which corresponds to the asymptotic region of the phase shift in Fig. 4a. Thus provided that intermittent contact is fully established at large vibrational amplitudes, the data suggest that the friction is relatively independent of the absolute value of the Young?s modulus. However, at smaller vibrational amplitudes, an increase in tc due to a reduction in the normal stiffness is more important than the corresponding reduction in the lateral stiffness. This is because the unloading distance of the normal spring starts to become comparable with amplitude of vibration and the system tends towards the transition regime or full contact (Fig. 4)). In the case of the normal force dependency (Fig. 9d), an increase in the normal force increases the lateral force required to induce slip. However, the increase of the static compression of the normal spring with increasing normal force causes an increase in tc. Consequently, there is a reduction in the rate at which the lateral force increases so that the integral frictional work is approximately constant. Again this effect is more dominant for $w > 2.5$. In both cases, it is important to emphasise that the frictional work is greatest when t_c is relatively short since the friction is governed by the intrinsic value of the finger pad. However, when t_c is relatively long, the friction is dominated by the smaller force required to deform the finger pad laterally.

5 DISCUSSION

5.1 Hypothesis and Results Analysis

A combination of experiment and modelling was employed in the current work to investigate the role of intermittent contact. Laser Doppler vibrometry data, which quantified the velocity of displacement of a finger pad and an ultrasonic device, showed that there was an increase in the phase shift, $\Phi(w)$, with increasing vibrational amplitude. At small amplitudes, the finger pad and the plate are in phase but there is an increase in the phase shift with increasing amplitude. For extreme vibrational amplitudes (2.5 µm peak-to-peak in the current work), a doubling of the contact period was observed, in accordance with the measurements performed by Dai et al [9]. The effect is more pronounced for the finger pad in the dry state for which the *stratum corneum* is less plasticised by moisture and hence stiffer than in the moist state. The analysis of the period doubling is outside of the scope of this paper, which is focussed on the main mechanism leading to the friction modulation. The transition from persistent or sticky contact to the intermittent or bouncing contact in state occurs at a peak-to-peak amplitude range of 0.4 - 0.8 µm compared with 0.8 - 1.3 µm for the moist state. The FE simulations involved a larger value of the Young's modulus of the *stratum corneum* for the dry compared with the moist state. On this basis it was possible to capture the observed trends of the measured phase shift data as shown in Fig. 4(a). The developed model suggests that immobility in the time scale of the oscillations could be applied. Recent studies involving different artificial fingertips suggested that the viscoelasticity of the subcutaneous tissues plays a fundamental role in reducing the friction [10], [11], while the behaviour as a function of vibrational frequency suggests effectively an immobile in the time scale of the oscillations response of the finger pad at the high frequencies associated with ultrasonic devices [28].

This is consistent with the assumption made in the current work that the preloading of the inner tissue is treated as irreversible within the timescale of the vibrations.

The input parameters for the FE model were optimised to reproduce the behaviour on the finger pad as represented by the measured phase shift data. The sliding results confirmed that the developed model exhibits a reduction in friction while sliding on an ultrasonic vibrating plate. Consequently we can deduce that a purely mechanical interaction can explain the friction reduction associated with ultrasonic vibration.

The squeeze film effect is the classic explanation of the friction modulation for ultrasonic devices. It relies on a net increase in the air pressure to decrease the friction. The limitations of this mechanism have been discussed in [8] with respect to the prediction that the friction tends to zero with increasing vibrational amplitude at a value of ~ 2 µm rather than to the finite value that is observed experimentally at a corresponding amplitude and frequency. For a finger pad in contact with an ultrasonically vibrating plate, it has been observed by optical reflection measurements that the amplitude of brightness is periodic [29], which is consistent with the temporal variation in the calculated normal force (Fig. 7) that governs the contact area. However, although the amplitude of brightness increased with increasing vibrational amplitude, the mean value decreased. This was interpreted as evidence of a squeeze film mechanism. Moreover, it showed that considering the interfacial roughness of the skin within the squeeze film effect modeling may explain the asymptotic behavior of the friction reduction. However, (i) it would be expected that the reduction in friction would be independent of the sliding velocity, (ii) dependent on the normal force applied, and (iii) independent on the vibrational frequency, which contradict the results of our current modelling and the experimental data reported in part 2. Given the computational complexity, the current modelling did not include the role of air, but it is reasonable to argue that the squeeze film mechanism is synergistic with the ratchet mechanism proposed in the current work since both mechanisms involve intermittent contact. The two mechanism may be synergistic in the sense that the skin asperities remaining in contact resulting from the force applied by the squeeze film effect experiences the frictional ratchet phenomenon.

To highlight the governing parameters of the interaction and facilitate an understanding of the principle, a massless spring-slider model is hereby introduced.

5.2 Dimensionless Group

A dimensionless group is useful for summarising the governing parameters of a system and allowing data superposition. A necessary condition for $\mu' < 1$ is that $t' < 1$ where $t' = t_c/T$. Then μ' depends on the ratio $\Psi = t_c/t_s$. It is not possible to write a closed-form solution for the current system and thus any dimensionless group that is derived will be accurate to first order, such as $t_c \approx F_{reac}/(k_n w)T = F_{reac}/(k_n wf)$ and $t_s \approx F_{reac}\mu_0/k_l U$. Thus the dimensionless group Ψ may be written as:

$$\Psi = \frac{F_{reac}}{k_n wf}\frac{k_l U}{F_{reac}\mu_0} = \frac{k_l U}{k_n wf\mu_0} \qquad (16)$$

Since for a finger pad, a common contact area for the two springs is involved [30], Eq. (16) may be written as:

$$\Psi = \frac{G_{sc}U}{E_{sc}wf\mu_0} = \frac{U}{wf\mu_0(1+\nu)} \tag{17}$$

A first order rate equation provides the simplest scheme for data superposition, i.e. it is an empirical equation that defines the rate of change of the coefficient of friction with respect to the dimensionless group:

$$\frac{d\mu}{d\Psi} = b(\mu_0 - \mu) \tag{18}$$

where b is a system constant. Eq. (18) may be written in terms of the relative coefficient of friction as follows:

$$\frac{d\mu'}{d\Psi} = b(1 - \mu') \tag{19}$$

By integrating subject to the boundary condition $\mu' = 0$ at $\Psi = 0$, the solution may be written in the following form:

$$\mu' = [1 - \exp(-\Psi/\Psi^*)] \tag{20}$$

where Ψ^* is the characteristic value of Ψ. The data in Fig. 9 change systematically with the independent variables except for the Young's modulus of the *stratum corneum* (Fig. 9b) and the applied normal force (Fig. 9d) which converge to single trend lines with increasing amplitude. At smaller amplitudes, it may be concluded that the relative friction is sensitive to the compressive displacement, as governed by the normal stiffness or applied normal force, since the intermittent contact is in the transition regime. Fig. 12 shows a plot of μ' as a function of Ψ and the best fit to Eq. (20) with $\Psi^* = 2.38 \pm 0.21$. The data correspond to those in Fig. 9 for a range of vibrational amplitudes, frequencies, exploration velocities, and intrinsic coefficients of friction. It also includes data for the Young's moduli and applied normal forces for amplitudes > 1 μm; the data at smaller amplitudes diverge from the correlation since there is a significant dependence on these parameters that is not taken into account in the definition of the dimensionless group. Thus Eq. (20) provides a reasonable representation of the data in reduced variables, particularly given the wide range of each variable that has been included.

Fig. 12 provides fundamental design guidelines for ultrasonic tactile devices. To obtain a large reduction of friction, small values of the dimensionless group are required. Thus, accounting for (19), it is possible to understand that the relevant parameters are (i) the vibrational amplitude as is well known, but also (ii) the vibrational frequency, and (iii) the intrinsic friction coefficient. The other parameters, exploration velocity, skin parameters, and normal load, are not controllable by a device designer. The influence of these parameters on the energetic consumption of such devices are beyond the scope of this paper. However, as suggested in [31] the dependence of the power consumption of the plate, among other parameters, is a function of the vibrational frequency and the quadratic value of the vibration amplitude. On the other hand, the developed model shows that the friction reduction is linearly dependent on the product of vibrational amplitude and the frequency (wf). We can deduce that the frequency should be a more effective parameter to improve the friction reduction considering the power consumption issues.
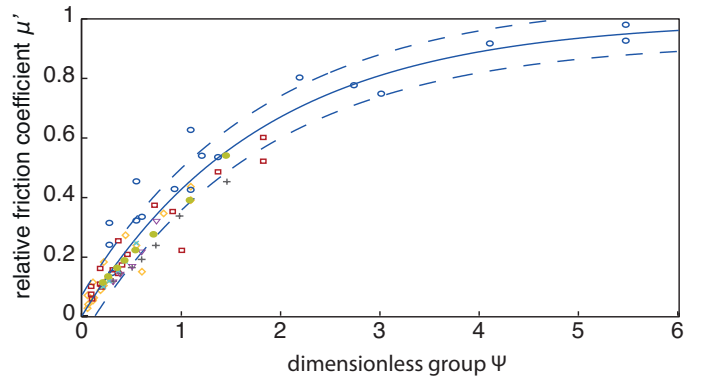

Fig. 12: Relative coefficient of friction as a function of the dimensionless group, $U/wf\mu_0(1+\nu)$, for peak-to-peak vibrational amplitudes, w, of 1 (blue circles), 3 (red squares), and 5 μm (yellow diamonds), applied normal forces, F_n, of 0.1 (full green dots) and 1 N (light blue crosses), Young's moduli, E_{sc}, of 20 (purple triangles) and 50 MPa (grey crosses) frequencies in the range f =10 - 100 kHz, sliding velocities in the range U = 5 - 100 mm/s, and intrinsic coefficients of friction in the range = 0.1 - 2. Unless indicated, μ_0 = 0.5, U = 20 mm/s, f = 27.5 kHz, E_{sc} = 28.3 MPa and F_n = 0.5 N. The dashed blue lines correspond to the RMSE of the fit (continuous line). The data are taken from Fig. 9 with those for the Young's modulus and applied normal force at amplitudes < 1 μm being omitted.

5.3 Influence of the Viscoelasticity

Both the current FE and spring-slider models demonstrate that it is not necessary to invoke viscoelastic deformation of the ridges to account for the reduction in friction. However, the optical measurements and the FE results (Fig. 5) show that inertia has a significant effect on the unloading and it may be speculated that a component of the measured damping arises from viscoelasticity, which could also retard the lateral recovery of the ridges following loss in contact. The aim of this section is to examine the influence of viscoelasticity on the reduction in friction. While a spring-dashpot-slider model could be developed, albeit with the introduction of increased complexity and additional input parameters, it is straightforward to examine the effect of retarding the recovery of the lateral spring by incorporating a constant unloading velocity as shown in Fig. 13. Initially, the effect is relatively large but there is an accumulation of the pre-contact unloaded lateral displacement that results in a transient increase in the friction to an asymptotic value that is slightly less than that corresponding to slip for the whole contact duration, $\mu_0 F_{reac}$. These calculations were extended to a range of exploration velocities. The results show that the steady state relative coefficient of friction decreases with increasing unloading velocity at a given vibrational amplitude (Fig. 14). This is expected since the steady state pre-contact residual deformation will also decrease with increasing unloading velocity. Thus, although gross viscoelastic damping of the finger pad is a necessary condition
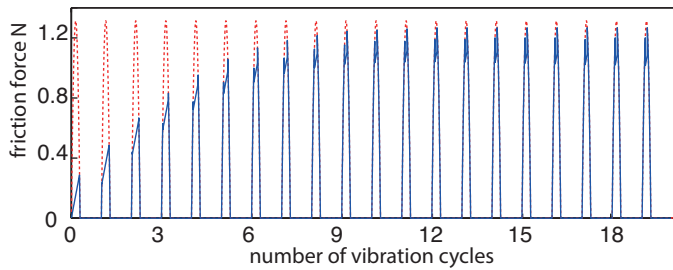
Fig. 13: The frictional force as a function of the number of vibrational cycles with a lateral skin recovery speed of 1.5 mm/s (continuous blue line) as calculated by the spring-slider model with normal and lateral spring stiffnesses of 3.9 and 1.5 MN/m, a vibrational amplitude of 5 μm, a normal load of 0.5 N, static friction coefficient of $\mu_0 = 0.5$ and plate sliding velocity of 20 mm/s. The dotted red line shows the results for an infinitely fast recovery speed as calculated from $\mu_0 F_{reac}$.
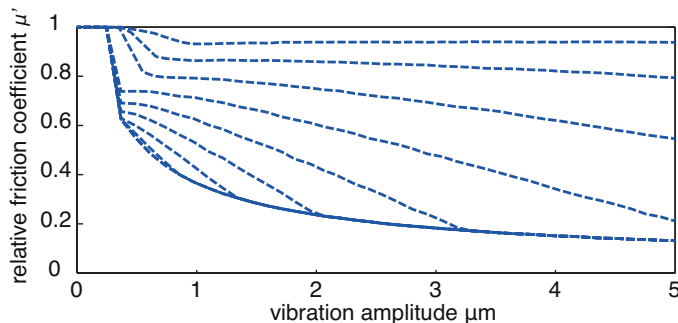

Fig. 14: The steady state relative coefficient of friction as a function of the vibrational amplitude calculated using the spring-slider model with the input parameters equal to those in Fig. 13 except that lateral recovery velocity of the skin was varied between 1.5 (top line) to 15 mm/s (lower line).

to achieve a friction modulation, lateral damping of the external layers of the skin causes a reduced modulation. The results of this analysis are in accord with the inverse analysis performed on the FE model which confirmed that the external layer of the skin can be considered elastic in the ultrasonic regime.

5.4 Contribution of Other Phenomena

Another application of the developed mechanical model is to allow the analysis of different mechanisms proposed in the literature explaining the friction reduction provided by ultrasonic devices: the de-occlusion mechanism, stochastic adhesion theory and non-Coulombic friction [30], in addition to the potential role of the squeeze film effect, which will be considered in part 2 [14]. De-occlusion may result in a hardening of the skin after each loss of contact. It would arise from the partial drying of the most external layer of the skin, compared to the extent of hydration corresponding to a finger pad in a sustained contact, which generates a harder impact, and a possible consequent smaller contact area, at every cycle of vibration. However, the evidence from the current work suggests that any such small change in

the Young's modulus would not have a major effect on the friction. It is also consistent with the findings that ultrasonic vibration reduces the friction of solids having a wide range of Young's moduli, for example, from tens of kPa [32] to hundreds of GPa [33]. The stochastic adhesion mechanism could contribute to the reduction in the friction. It relies on the regeneration of the population molecular bonds at the interface following a loss in contact. The friction of the fingerpad sliding on a surface may be described by considering the total number of interface molecules interacting between the two bodies, after the generation of the intermittent contact; this population is disrupted at each cycle of vibration. To obtain a significant effect, it requires that the repinning time of the bonds is short compared with the smallest contact duration; more details about the stochastic adhesion theory applied to the finger pad can be found in [17]. However, the ubiquitous nature of the influence of ultrasonics on friction modulation would suggest that the contribution would be second order if it were significant. The input parameters for the FE analysis were optimised for a system that was independent of the dwell time of contact and thus not considered in the current work. The friction of a finger pad is non-Coulombic against smooth surfaces, which could enhance the reduction in friction. This aspect will be considered in part 2 [14].

6 CONCLUSION

In this paper, a finite element model of the fingerprint ridges was developed and calibrated through an inverse analysis of experimental measurements. With this model the parametric dependence of the reduction of the friction generated by the mechanical interplay between a vibrating plate and a finger was highlighted. The main results of the modelling suggest that: (i) intermittent contact is the dominant mechanism for the friction modulation associated with ultrasonic displays, (ii) the phenomenon is systematically dependent on the vibrational amplitude and, frequency, intrinsic friction coefficient, and exploration velocity, and (iv) it is independent on the applied normal force and the mechanical properties of the skin, provided that the intermittent contact is sufficiently well developed. An analytical model was then developed to further perform the parametric analysis and propose a dimensionless group dependent on the governing parameters to provide design guidelines and allow data superposition. Finally, the potential contribution of the stochastic adhesion mechanism and the de-occlusion mechanism was considered but it was concluded that they do not make a significant contribution. In part 2 [14], The experimental assessment of the current model for *in vivo* and probe tribological measurements will be performed, as well as the quantification of the contribution of the squeeze film effect and non-Coulombic friction to the reduction of friction. In summary, a reliable theoretical model of the friction modulation for ultrasonic devices will have implications for control, energy consumption and performance optimisation. The introduction of an open-loop control of the lateral force, based on this model, will assist in increasing the fidelity of the simulation of textures and objects.

REFERENCES

[1] M. Wiertlewski, J. Lozada, and V. Hayward, "The spatial spectrum of tangential skin displacement can encode tactual texture," *IEEE Transactions on Robotics*, vol. 27, no. 3, pp. 461–472, Jun. 2011.

[2] M. Biet, G. Casiez, F. Giraud, and B. Lemaire-Semail, "Discrimination of virtual square gratings by dynamic touch on friction based tactile displays," in *Symposium on Haptic Interfaces for Virtual Environment and Teleoperator Systems*, Mar. 2008, pp. 41–48.

[3] E. Mallinckrodt, A. L. Hughes, and W. Sleator, "Perception by the skin of electrically induced vibrations," *Science*, vol. 118, no. 3062, pp. 277–278, 1953.

[4] E. Vezzoli, M. Amberg, F. Giraud, and B. Lemaire-Semail, "Electrovibration modeling analysis," in *Haptics: Neuroscience, Devices, Modeling, and Applications*, ser. Lecture Notes in Computer Science, M. Auvray and C. Duriez, Eds. Springer Berlin Heidelberg, Jan. 2014, pp. 369–376.

[5] E. Vezzoli, W. B. Messaoud, M. Amberg, F. Giraud, B. Lemaire-Semail, and M. A. Bueno, "Physical and perceptual independence of ultrasonic vibration and electrovibration for friction modulation," *IEEE Transactions on Haptics*, vol. 8, no. 2, pp. 235–239, April 2015.

[6] M. Biet, F. Giraud, and B. Lemaire-Semail, "Squeeze film effect for the design of an ultrasonic tactile plate," *IEEE Transactions on Ultrasonics, Ferroelectrics, and Frequency Control*, vol. 54, no. 12, pp. 2678–2688, Dec. 2007.

[7] T. Watanabe and S. Fukui, "A method for controlling tactile sensation of surface roughness using ultrasonic vibration," in *IEEE International Conference on Robotics and Automation, 1995. Proceedings.*, vol. 1, pp. 1134–1139 vol.1.

[8] T. Sednaoui, E. Vezzoli, B. Dzidek, B. Lemaire-Semail, C. Chappaz, and M. Adams, "Experimental evaluation of friction reduction in ultrasonic devices," in *2015 IEEE World Haptics Conference (WHC)*, June 2015, pp. 37–42.

[9] X. Dai, J. Colgate, and M. Peshkin, "LateralPaD: A surface-haptic device that produces lateral forces on a bare finger," in *2012 IEEE Haptics Symposium (HAPTICS)*, Mar. 2012, pp. 7–14.

[10] R. F. Friesen, M. Wiertlewski, M. A. Peshkin, and J. E. Colgate, "Bioinspired artificial fingertips that exhibit friction reduction when subjected to transverse ultrasonic vibrations," in *2015 IEEE World Haptics Conference (WHC)*, June 2015, pp. 208–213.

[11] R. F. Friesen, M. Wiertlewski, and J. E. Colgate, "The role of damping in ultrasonic friction reduction," in *2016 IEEE Haptics Symposium (HAPTICS)*, April 2016, pp. 167–172.

[12] M. . Biet, "Conception and control of electro-active motors for tactile stimulation," *PhD Thesis - Lille University*.

[13] D. T. Pawluk and R. D. Howe, "Dynamic contact of the human fingerpad against a flat surface," *Journal of Biomechanical Engineering*, vol. 121, no. 6, pp. 605–611, Dec. 1999.

[14] T. Sednaoui, E. Vezzoli, B. Dzidek, B. Lemaire-Semail, C. Chappaz, and M. Adams, "Friction reduction through ultrasonic vibration part 2: Experimental study to evaluate intermittent contact and squeeze film levitation," *Submitted to IEEE Transaction on Haptics*, 2016.

[15] G. Imokawa, S. Akasaki, Y. Minematsu, and M. Kawai, "Importance of intercellular lipids in water-retention properties of the stratum corneum: induction and recovery study of surfactant dry skin," *Archives of Dermatological Research*, vol. 281, no. 1, pp. 45–51, Feb. 1989.

[16] G. Imokawa and M. Hattori, "A possible function of structural lipids in the water-holding properties of the stratum corneum," *Journal of Investigative Dermatology*, vol. 84, no. 4, pp. 282–284, Apr. 1985.

[17] M. J. Adams, S. A. Johnson, P. Lefèvre, V. Lévesque, V. Hayward, T. André, and J.-L. Thonnard, "Finger pad friction and its role in grip and touch," *Journal of The Royal Society Interface*, vol. 10, no. 80, 2012.

[18] H. Fruhstorfer, U. Abel, C. D. Garthe, and A. Knüttel, "Thickness of the stratum corneum of the volar fingertips," *Clinical Anatomy (New York, N.Y.)*, vol. 13, no. 6, pp. 429–433, 2000.

[19] J. v. Kuilenburg, M. A. Masen, and E. v. d. Heide, "Contact modelling of human skin: What value to use for the modulus of elasticity?" *Proceedings of the Institution of Mechanical Engineers, Part J: Journal of Engineering Tribology*, vol. 227, no. 4, pp. 349–361.

[20] T. Vodlak, Z. Vidrih, D. Fetih, D. Peric, and T. Rodic, "Development of a finite element model of a finger pad for biomechanics of human tactile sensations." Milano, Italy: IEEE EMBC, 2015, accepted as a technical paper.

[21] T. Belytschko, J. S.-J. Ong, Wing Kam Liu, and J. M. Kennedy, "Hourglass control in linear and nonlinear problems," *Computer Methods in Applied Mechanics and Engineering*, vol. 43, no. 3, pp. 251–276, May 1984.

[22] P. Wriggers, *Computational Contact Mechanics*. Berlin, Heidelberg: Springer Berlin Heidelberg, 2006.

[23] K. L. Johnson, *Contact Mechanics*. Cambridge University Press, Aug. 1987.

[24] B. M. Dzidek, M. Adams, Z. Zhang, S. Johnson, S. Bochereau, and V. Hayward, "Role of occlusion in non-coulombic slip of the finger pad," in *Haptics: Neuroscience, Devices, Modeling, and Applications*. Springer Berlin Heidelberg, 2014, vol. 8618, pp. 109–116.

[25] D. R. Einstein, A. D. Freed, N. Stander, B. Fata, and I. Vesely, "Inverse parameter fitting of biological tissues: a response surface approach," *Annals of Biomedical Engineering*, vol. 33, no. 12, pp. 1819–1830, Dec. 2005.

[26] F. Lei and A. Z. Szeri, "Inverse analysis of constitutive models: Biological soft tissues," *Journal of Biomechanics*, vol. 40, no. 4, pp. 936–940, 2007.

[27] A. Tarantola, *Inverse Problem Theory and Methods for Model Parameter Estimation*. SIAM, 2005.

[28] M. Wiertlewski and V. Hayward, "Mechanical behavior of the fingertip in the range of frequencies and displacements relevant to touch," *Journal of Biomechanics*, vol. 45, no. 11, pp. 1869–1874, 2012.

[29] M. Wiertlewski, R. Fenton Friesen, and J. E. Colgate, "Partial squeeze film levitation modulates fingertip friction," *Proceedings of the National Academy of Sciences*, vol. 113, no. 33, pp. 9210–9215, 2016.

[30] E. Vezzoli, B. M. Dzidek, T. Sednaoui, F. Giraud, M. Adams, and B. Lemaire-Semail, "Role of fingerprint mechanics and non-coulombic friction in ultrasonic devices," *WHC 2015*.

[31] Y. Yang, B. Lemaire-Semail, F. Giraud, M. Amberg, Y. Zhang, and C. Giraud-Audine, "Power analysis for the design of a large area ultrasonic tactile touch panel," *Eur. Phys. J. Appl. Phys.*, vol. 72, no. 1, p. 11101, 2015.

[32] Z. Huang, M. Lucas, and M. J. Adams, "Influence of ultrasonics on upsetting of a model paste," *Ultrasonics*, vol. 40, no. 1-8, pp. 43–48, May 2002.

[33] Y. M. Huang, Y. S. Wu, and J. Y. Huang, "The influence of ultrasonic vibration-assisted micro-deep drawing process," *The International Journal of Advanced Manufacturing Technology*, vol. 71, no. 5-8, pp. 1455–1461, Jan. 2014.

Eric Vezzoli got his MS degree in Physics Engineering from the Politecnico of Milan (Italy) in 2013. From September 2013 he is research assistant at L2EP-IRCICA Laboratory working on his PhD Thesis with the ITN Prototouch Project. His domain of research are tactile stimulation principle modelling, tactile display designing and tactile perception.

Zlatko Vidrih was awarded a PhD in 2012 in Earthquake Engineering by The Institute of Structural Engineering, Earthquake Engineering and Construction IT. He worked as a postdoctoral researcher on NanoBioTouch project at Faculty of Natural Sciences and Engineering, Ljubljana, Slovenia, and Prototouch project at College of Engineering, Swansea, UK.

Vincenzo Giamundo received the Ph.D. degree in Materials and Structures in 2014 from the University of Naples Federico II, (Italy). Form 2015, he started working at the C3M - Centre for Computational Continuum Mechanics (Slovenia) as experienced researcher in the ITN Prototouch Project. His research currently deal with computational biomechanics and tactile stimulation mechanical modelling.

Betty Lemaire-Semail received the Ph.D. degree in 1990 from the University of Paris XI, Orsay. From 1990 to 1998, she was an assistant professor at the Ecole Centrale of Lille and she is now a professor at the University Lille 1. Her main field of interest now deals with the modeling and control of piezoelectric actuators for positioning and force feedback applications.

Frederic Giraud received the Ph.D. degree in 2002 in electrical engineering from the University lille 1 where he is now associate professor. His research deals with the modeling and control of piezoelectric actuators.

Tomaz Rodic received the Ph.D. degree from the University of Wales, Swansea, UK. Currently he is full professor for the area of Engineering Materials at University of Ljubljana, SI, Faculty for Natural Sciences and Engineering and director of the Slovenian Centre of Excellence for Space Sciences and Technologies SPACE-SI and Centre for Computational Continuum Mechanics C3M. His main research area is numerical modelling of M5 (Multi-field, Multi-scale, Multi-body, Multi-phase & Multi-objective) systems in converging sciences and engineering.

Djordje Peric was awarded a PhD in computational mechanics in 1992 from the Swansea University, UK and has held a Personal Chair at the Swansea University, UK since 2000. He is a Fellow of the International Association for Computational Mechanics and Learned Society of Wales. His research focuses on development of computational methods for solid, fluids and coupled systems.

Michael Adams was awarded a PhD in molecular acoustics from the University of Essex, UK and is Professor of Product Engineering and Manufacturing in the School of Chemical Engineering at the University of Birmingham, UK since 2004 and was previously a Senior Scientist with Unilever R&D. He is a Fellow of the UK Royal Academy of Engineering. He was the recipient of the Donald Julius Groen Prize (IMechE) for outstanding achievements in interfacial engineering. His research interests include the friction of human skin and applications to tactile sensors and displays.